Strain, interdiffusion, and microstructural evolution under ion irradiation in Ni(111)/Mo(110) multilayers: Interdependence with elastic properties

F. Martin, C. Jaouen,* J. Pacaud, and G. Abadias
Laboratoire de Métallurgie Physique, UMR CNRS 6630, Université de Poitiers, SP2MI, Av. M. et P. Curie, BP 30179, 86962 Futuroscope-Chasseneuil Cedex, France

Ph. Djemia and F. Ganot†
Laboratoire des Propriétés Mécaniques et Thermodynamiques des Matériaux, UPR CNRS 9001, Université Paris-Nord, Avenue J.B. Clément, 93430 Villetaneuse, France

(Received 17 May 2004; revised manuscript received 5 October 2004; published 24 January 2005)

The interdependence between the microstructure of sputter-deposited Ni(111)/Mo(110) superlattices and their elastic behavior is investigated as a function of the bilayer period (Λ). Brillouin light scattering measurements show that a drastic softening of the effective shear modulus occurs with decreasing Λ, until $\Lambda = 2$ nm where it reaches −62%. Ion irradiation is here used to trigger stress relaxation and to induce, in a controlled way, interdiffusion and structural changes allowing us thus to investigate their influence on the elastic anomaly. At a very low irradiation dose (0.1 displacements per atom), the relief of the lattice expansion and associated compressive stresses does not induce any change of the elastic response, which indicates that the elastic behavior of the as-grown multilayers is not correlated with the presence of elastic strains. Furthermore, a detailed x-ray diffraction analysis shows that the unstrained lattice parameter of Mo layers exhibit a linear dependence with the interface density, while the Ni unstrained lattice parameter remains nearly unchanged in the same Λ range. This effect can be attributed to an interfacial mixing of a constant Ni amount (~1.5 monolayers) into the Mo layers, as a consequence of a dynamic segregation of Ni atoms during growth. Thus, the formation of interfacial metastable and supersaturated solid solutions, structurally and mechanically unstable, appears as the origin of the huge elastic softening observed in this system. At high ion fluences, when the mixing process becomes dominant, the present study also provides experimental data on phase transformation in "driven" alloys, by addressing the issue of the stability of out-of-equilibrium structures under irradiation.

DOI: 10.1103/PhysRevB.71.045422 PACS number(s): 68.65.Ac, 68.60.Bs, 61.80.Jh, 68.35.Dv

I. INTRODUCTION

It is now well known that interesting and unexpected physical properties departing from the bulk properties are currently observed for artificially layered systems when layer thicknesses are reduced to the nanoscale. The mechanical behavior of metallic superlattices does not provide an exception and has been the subject of much interest and controversy in the recent years.[1,2] The presence of deviations in the elastic behavior of some multilayered systems, compared to what continuum elasticity predicts, has given rise to the development of considerable experimental and theoretical studies. A strong hardening involving an increase of the in-plane biaxial modulus of more than 100%, referred historically as the "supermodulus" effect, has been seen in some fcc/fcc systems[3–5] from bulge-test techniques. Although this effect has been later refuted and ascribed to some artifacts in the experimental measurements, it is, however, well recognized that significant elastic anomalies do exist in some peculiar bcc/fcc systems (Cu/Nb,[6–8] V/Ni,[9] Mo/Ni,[10–13] W/Ni,[14] Fe/Cu,[15] etc.) and more scarcely in bcc/bcc [Mo/Ta (Ref. 16)] or fcc/fcc [Ag/Pd (Ref. 17), Ag/Ni (Refs. 18 and 19)] systems. A strong softening (≈30–50%) of the effective shear modulus with decreasing bilayer period (Λ) of the superlattices is usually observed; this effect sometimes coexists with a slight stiffening (~10%) of the in-plane Young and biaxial effective moduli. It is also noteworthy that such an elastic behavior mostly occurs in systems for which constituents exhibit a large lattice mismatch and are rather immiscible, i.e., systems for which incoherent and sharp interfaces are expected. In very rare instances and more especially in miscible fcc/fcc systems (Ag/Pd), strong hardening is reported for both the shear and biaxial effective moduli.[17]

Quantitative structural information on lattice strains and structural disorder has been mainly obtained from analysis of x-ray scattering in specular or grazing geometries. To determine the out-of-plane interplanar spacings of the constituent layers, it is necessary to fit the diffraction spectra to model calculations. Experimentally, it has been reported that the softening of the shear (C_{44} elastic constant) and compressional (C_{33} elastic constant) moduli was correlated with an expansion of the average interplanar spacing along the growth direction[10,12] ($\bar{d}$) and also possibly with an increased structural disorder at the interfaces able to trigger a crystalline to amorphous transition at small Λ.[10,14] Different theoretical models involving either (i) bulk lattice deformations induced by a modified band structure due to the artificial periodicity[20,21] or by the difference in the Fermi energy level between the two metallic layers,[22] (ii) a localized strain due to interface stresses at noncoherent interfaces[23,24] or (iii) coherency strains,[25,26,15] have been proposed to correlate the elastic response to different electronic or structural mecha-

nisms. Finally, Wolf and co-workers have developed a model based on the idea of "grain boundary" interfaces and related atomic-level disorder,[27–29] which allowed them to account for both shear elastic softening and biaxial modulus enhancement observed in some systems. The role of the interfaces in governing the elastic behavior of nanoscale metallic superlattices is now well determined, but their intrinsic nature and the underlying physical mechanisms are not yet well understood.

The Ni/Mo system has been extensively studied[10,12,30] and exhibits the largest elastic anomalies of any system reported in the literature. For instance, a large softening of the C_{44} shear modulus ($\sim -44\%$) and C_{33} compressional modulus ($\sim -33\%$) has been observed by Khan *et al.*[10] and Clemens and Eesley[12] at small Λ, in Ni/Mo multilayers grown by magnetron sputtering. However, the physical origin is still subject to controversy since contradictory conclusions have been drawn: Clemens and Eesley claimed that the commonly observed expansion of $\bar{d}$ was localized at the interface,[12] while Khan *et al.*[10] and Schuller and Raman[31] have ascribed it to a bulk strain in the Ni lattice, arising from a bulk relaxation attributed to electronic transfer effects. Finally, through a complete determination of the stress state of the two constituents, Bain *et al.*[32] demonstrated that the observed out-of-plane lattice expansion was completely accounted for by elastic strains arising from coherency and substrate-interaction stresses, ruling out implicitly the interface contraction stresses and associated dilatation strains as the causes for the shear elastic softening in Ni/Mo superlattices. Considering these conflicting explanations, we have first undertaken an investigation to reexamine the Ni/Mo system. For this purpose, a detailed structural characterization by x-ray Diffraction (XRD) coupled with Brillouin light scattering (BLS) measurements was carried out in sputtered Ni/Mo multilayers, with Λ ranging from 0.8 to 87.5 nm.[33]

The originality of the present study lies in the use of the ion-irradiation technique as a powerful tool to induce, in a controlled way, structural changes and to investigate how they relate to the elastic properties. Irradiation was performed using 380 keV Ar ions in a large range of fluences to study the influence of stress relaxation and ion-driven interdiffusion on the evolution of the shear elastic modulus. By combining the structural and elastic investigation techniques with ion irradiation, we obtain a complete characterization of the interplanar spacings as a function of Λ for the as-deposited and irradiated samples, and show that the huge softening of the shear modulus (-62%) is not related to an expansion of $\bar{d}$, as stated previously,[1,10,12,15] but rather correlated with structural changes in the individual Mo and Ni sublayers due to an interfacial alloying effect. This picture is reinforced by recent results obtained on $Ni_{1-x}Mo_x$ supersaturated solid solutions elaborated by co-sputtering, for which a strong softening of C_{44} is observed as a function of the solute concentration.[33] The present study also provides experimental data on phase transformation in "driven" alloys, by addressing the issue of the stability of nonequilibrium structures.

II. EXPERIMENTAL DETAILS

A. Elaboration

The Mo/Ni multilayers were grown at room temperature (RT) on Si(001) substrates covered with a thin ($\sim$1–2 nm) native SiO_2 amorphous layer. Bilayer periods Λ ranged from 0.8 to 87.5 nm, with a constant Mo:Ni thickness ratio. The multilayered films were elaborated in a high-vacuum, computer-controlled Nordiko 3000 sputtering device fitted with a rf-plasma ion gun and two cryogenic pumps. The initial pressure in the deposition chamber was $1-2 \times 10^{-6}$ Pa, while the working pressure after Ar introduction was fixed at $\sim 10^{-2}$ Pa. The acceleration voltage and ion current were kept constant at 1.2 kV and 80 mA, respectively, resulting in a deposition rate of 0.06 and 0.082 nm s^{-1} for Mo and Ni, respectively. Total film thickness was $\sim$280 nm. The global composition of the film was chosen to be $Mo_{0.25}Ni_{0.75}$, which corresponds roughly to a Mo:Ni thickness ratio equal to 1:2. The exact composition was determined from energy dispersive x-ray spectroscopy measurements (EDX) carried out in a scanning electron microscope using an accelerating voltage of 20 kV.

B. X-ray diffraction

Structural characterizations were carried out on a Bruker D5005 x-ray diffractometer equipped with a graphite secondary beam monochromator (selecting the Cu K_α radiation $\lambda = 0.1542$ nm) and a proportional counter. Measurements were recorded in the Bragg-Brentano geometry. Scattering angular ranges used ($35° - 70°$ and $75° - 110°$) were chosen to cover both first and second scattering orders from the Ni(111) and Mo(110) Bragg reflections. The lack of any other reflection indicates that the multilayers are highly textured, with an alternate stacking of bcc Mo(110) and fcc Ni(111) dense planes. Moreover, the presence of the high-angle superlattice peaks indicates that the interfaces are crystalline even at the smallest Λ investigated. A determination of the exact values of Λ and $\bar{d}$ defined by

$$\bar{d} = \frac{N_{\mathrm{Mo}} d_{\mathrm{Mo}} + N_{\mathrm{Ni}} d_{\mathrm{Ni}}}{N_{\mathrm{Mo}} + N_{\mathrm{Ni}}} \tag{1}$$

can be obtained directly from the positions of the superlattice maxima, using the relation

$$q = m\frac{2\pi}{\bar{d}} \pm n\frac{2\pi}{\Lambda}, \tag{2}$$

where $N_{\mathrm{Mo(Ni)}}$ and $d_{\mathrm{Mo(Ni)}}$ are the number of atomic planes and the out-of-plane interplanar distance of the individual Mo or Ni sublayer, respectively, q is the modulus of the scattering vector $q = 4\pi \sin\theta/\lambda$, m the scattering order and n the peak index. So, the zero-order peak ($n=0$) gives directly $\bar{d}$.

The information on the structural parameters of the individual constituent layers requires modeling the multilayer and a refinement procedure, which compares the calculated intensities from the model structure with the measured inten-

sities. Here, the kinematic model SUPREX was used.[34] No interdiffusion profile was introduced at the interfaces; thus, only *average* structural parameters of the individual Mo and Ni layers were determined. For Λ ranging from 4.3 to 10.8 nm, the simultaneous adjustment of the first-and second-order XRD profiles provides good accuracy on the values of the average interplanar spacing, d_{Ni} and d_{Mo}, and number of atomic planes, N_{Ni} and N_{Mo}, and gives a reliable determination of these values. For large periods ($\Lambda > 14$ nm), when the structural coherency length becomes similar or lower than Λ, only the values of d_{Ni} and d_{Mo} could be reasonably deduced from the adjustments of the XRD spectra. Lastly, for small periods ($\Lambda < 4.3$ nm), only information on $\overline{d}$ and Λ could be extracted.

X-ray reflectometry (XRR) measurements were also carried out on a Seifert XRD 3000 diffractometer, using a Cu $K\alpha_1$ radiation selected by a channel-cut Ge(220) monochromator and a fine slit. XRR measurements were performed in the specular $\theta-2\theta$ configuration, using a knife device to maintain a constant irradiated area on the specimen surface throughout the whole scan. The data were analyzed on the basis of Parrat's recursive formalism.[35] Therefore, quantitative information on Λ, the layer refractive index, interface roughness, and thickness ratio could be extracted.

C. Ion irradiation

Ni/Mo multilayers were subsequently irradiated at RT with 380 keV Ar ions, in another chamber with a vacuum of $\sim 10^{-5}$ Torr. The ion current was always maintained below 0.8 μA/cm^2 in order to avoid any sample heating. The ion energy was selected so that the profile of displaced atoms, deduced from SRIM simulations,[36] was as flat as possible throughout the whole multilayer thickness. An average dose of 0.14 displacements per atom (dpa) could be estimated for a fluence of 10^{14} Ar/cm^2, by referring to the displacement threshold energies of Mo and Ni.[37] A low fluence of 7×10^{13} ion/cm^2 (corresponding to 0.1 dpa) was first performed and, as previously shown,[38] was sufficient to induce an almost complete relaxation of the intrinsic stresses. Higher fluences, from 10^{14} to 10^{17} ions/cm^2, were also carried out on selected multilayers, $\Lambda = 2.8$, 7.7, and 28.4 nm, in order to follow the structural and elastic properties during the progressive interfacial mixing and until the formation of a final homogeneous solid solution.

D. Brillouin light scattering

BLS measurements were used to determine the phase velocity of the surface acoustic waves. The spectra were recorded in air at RT by means of a high-contrast Sandercock-type tandem (3+3 passes) Fabry-Perot interferometer. A single-mode Ar^+ laser ($\lambda = 514.5$ nm) of $\sim$400 mW power, polarized in the incidence plane, was focused onto the sample surface. Measurements were recorded in the backscattering interaction geometry for two incidence angles (65° and 45°). Since the acoustic wavelengths (typically 300 nm) are large compared to Λ, the elastic properties of the multilayered films can be described within the elastic continuum approximation. The set of elastic constants can in principle be determined by fitting the complete BLS spectra. It is assumed for the calculation that the ripple mechanism at the free surface is the only efficient one.[39]

The total thickness of the film required for the simulation of the BLS spectra was obtained from the refinement of the XRR profiles. The effective density (ρ) was obtained using the bulk densities of the two materials and the thickness ratio calculated from the global composition of the multilayers.

In the present case, among the five independent elastic constants that are necessary to describe the elastic hexagonal symmetry, only C_{11}, C_{33}, C_{13}, and C_{44} are related to the observed surface waves polarized in the sagittal plane. Nevertheless, an unambiguous determination is only possible for C_{44}.[18] The expected effective shear elastic constant of the superlattices, noted C_{44}^{ref}, was calculated from the respective C_{44} values of the two constituents, using the rule of the weighted harmonic average, accordingly the theoretical analysis of Grimsditch and Nizzoli.[40] Since the layers are polycrystalline in the plane (fiber-textured films), the C_{44} elastic constant has to be averaged over all possible in-plane orientations, which requires the use of a grain interaction model. Taking into account the observed texture, (111) and (110) for fcc Ni and bcc Mo layers, respectively, the corresponding values were calculated from the values of Ni and Mo single-crystal elastic constants,[41] using the Reuss[42] or Voigt averages[43] around the $\langle 111 \rangle$ and $\langle 110 \rangle$ axis, depending on whether the continuity of stress or strain across crystallite boundaries is assumed. Since it is usually observed that measured macroscopic values in thin textured films lie between the Reuss and Voigt values, the retained one was that calculated using the so-called Hill average,[44] which is a median value between the Reuss and Voigt estimates. This gives $C_{44}^{ref} = 79$ GPa.

III. RESULTS

A. As-deposited multilayers

1. Elastic properties

Figure 1(a) displays typical experimental and calculated BLS spectra of the as-grown multilayer with $\Lambda = 2.8$ nm recorded under an incidence angle of 65° in the as-deposited state. In this example, the Rayleigh surface mode (noted *R*) is fitted with $C_{44} = 32$ GPa, whereas a convenient fit of the so-called Sezawa modes is obtained with $C_{11} = 310$ GPa, $C_{33} = 320$ GPa, and $C_{13} = 151$ GPa. The evolution of the C_{44} effective elastic constant, deduced from the BLS measurements, is reported in Fig. 2 as a function of Λ. The expected C_{44}^{ref} value calculated using the Hill average is also reported. It appears that such a value is never reached, even for the largest Λ values where the influence of the interfaces is expected to be small. We ascribe this apparent reduction of C_{44} at large Λ (compared to C_{44}^{ref}) to an intrinsic elastic softening of the Mo sublayers. Indeed, a value of $C_{44} = 98$ GPa was measured for a pure Mo(110) thin film (thickness 200 nm), which is 23% lower than the bulk one (127 GPa). For small Λ values, a strong decrease of the shear modulus with Λ is clearly observed, reaching a lowest value of $C_{44} = 31$ GPa for

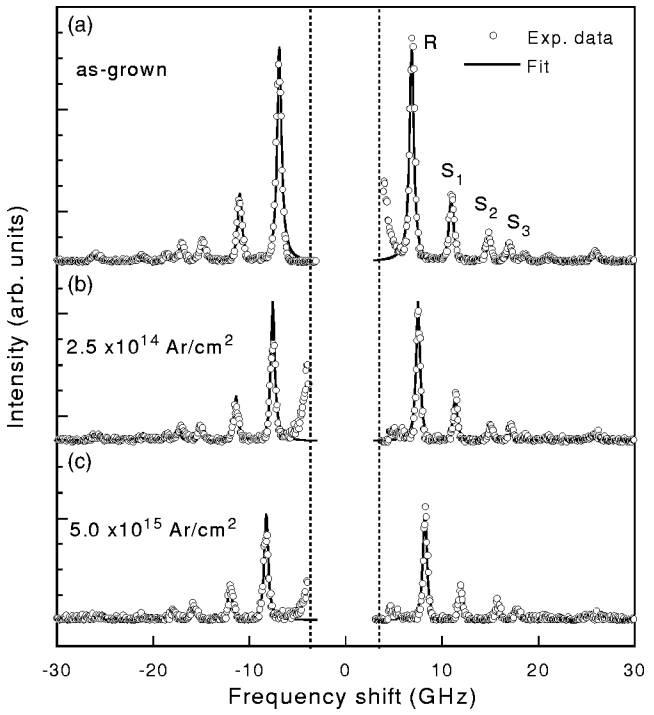

FIG. 1. Typical experimental BLS spectra (open symbols) compared with the calculated ones (solid lines) for a Ni/Mo multilayer with $\Lambda = 2.8$ nm (total thickness 288.4 nm, angle of incidence 65°): as-grown multilayer (a); irradiated with 2.5×10^{14} Ar/cm^2 (b); and 5×10^{15} Ar/cm^2 (c). The Rayleigh surface mode (noted *R*) is fitted with $C_{44} = 32$, 41, 51 GPa (the constants $C_{11} = 310$, 285, 285 GPa; $C_{33} = 320$, 325, 360 GPa; $C_{13} = 151$, 134, 134 GPa allow a convenient fit of the so-called Sezawa modes) for cases (a), (b), (c), respectively.

$\Lambda \leqslant 2$ nm. This latter value corresponds to a softening of $\sim 62\%$ with respect to the C_{44}^{ref} value. Such a behavior has also been reported previously by different groups;[10,12,30] however, in the present case, the Λ range where this softening is observed is much larger than that in previous studies, and the magnitude of the softening (-62%) is the highest ever reported. It is important to point out that the multilayers remain crystalline under the present deposition conditions even for $\Lambda < 2$ nm, and no increase in C_{44} is observed in this range (except however for the multilayer with $\Lambda = 0.8$ nm), contrary to a previous report.[10] The strong decrease of C_{44} with decreasing Λ clearly demonstrates the role of interfaces or more specifically of the interface density $(2/\Lambda)$. In a previous paper,[33] the remarkable linearity between $1/C_{44}$ and the interface density was seen, and a simple phenomenological model, based on a description of the system as parallel elastic layers, involving an extremely soft layer at each interface, was proposed. Adjustment of this model with the experimental data indicated a thickness of 1.2 nm and a C_{44} value of 31 GPa for this interfacial layer. This interpretation was supported by the drastic drop of C_{44} observed for crystalline $Ni_{1-x}Mo_x$ solid solutions elaborated by co-sputtering, when the induced solubility of Ni in Mo or of Mo in Ni is increased.

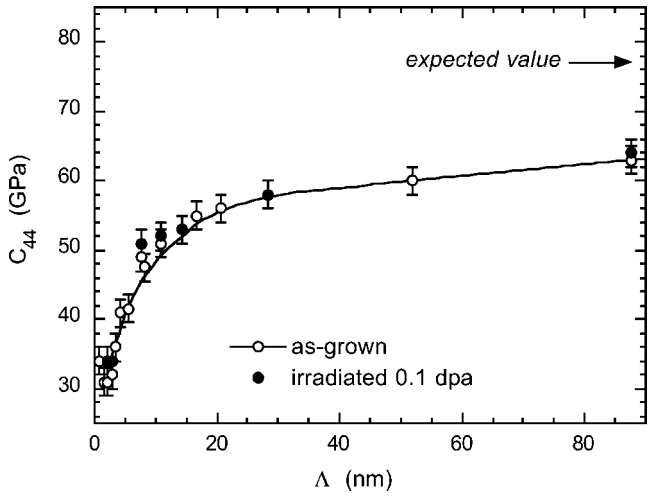

FIG. 2. Dependence of the shear elastic constant (C_{44}) as deduced from BLS measurements on superlattice bilayer period (Λ). Open symbols refer to as-grown multilayers and filled symbols to irradiated multilayers after a low ion fluence of 7×10^{13} Ar/cm^2 (0.1 dpa). The solid line is only a guide for the eyes.

2. XRD analysis

Representative XRD θ–2θ scans of Ni/Mo multilayered films with Λ ranging from 2 to 28.4 nm are shown in Fig. 3. As previously emphasized, the presence of superlattice reflections in the diffracted intensity indicates a rather good structural coherency, with a Ni(111)/Mo(110) stacking along the growth direction. For small Λ, the presence of satellite peaks is even preserved. These peaks are nevertheless wide due to a small grain size or a strong structural disorder. For large Λ, the overlapping of the superlattice peaks leads to their smearing out and disappearance. This is particularly visible at the second scattering order.

The main structural parameters were extracted following the procedure described in Sec. II B. Experimental and calculated profiles obtained for a multilayer with $\Lambda = 7.7$ nm are shown, for illustration, in Fig. 4. It is worth noticing that a good adjustment of the x-ray profiles to the kinematical model requires an apparent reduction of 25% of the Mo atomic diffusion factor. However, this effect appears fully accounted for by considering the larger mosaicity of the Mo planes compared to that of the Ni ones. Indeed, the full width at half maximum (FWHM) of the Mo (110) reflection in a ω-scan is systematically 1° larger than that of the Ni (111) reflection. Typical FWHM rocking curves values for Ni were in the range 4°–5° for Λ between 4 and 15 nm.

Figures 5 and 6 display the evolutions with Λ of d_{Mo} and d_{Ni} as well as $\delta\bar{d}/\bar{d}_{nom}$, where $\bar{d}_{nom}$ is the expected average value, calculated from the bulk lattice spacings, $d_{Mo}^{bulk} = 0.22254$ nm and $d_{Ni}^{bulk} = 0.20345$ nm, and the average numbers of Mo and Ni atomic planes, N_{Mo} and N_{Ni}. The values of d_{Mo}, d_{Ni}, and $\bar{d}$ are obtained from the refinement of the calculated spectra to fit the experimental ones. It may be pointed out that the value of $\bar{d}$ obtained from the fitting procedure is consistent with that obtained directly from the zero order Bragg reflection.

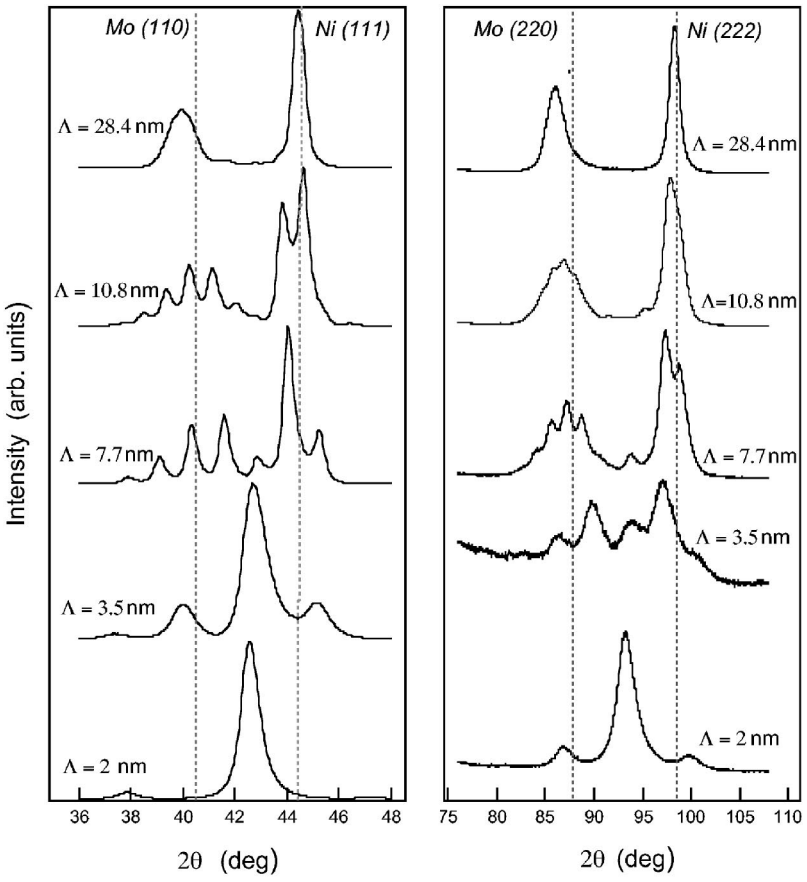

FIG. 3. High-angle symmetric θ-2θ XRD scans for representative Ni(111)/Mo(110) multilayers recorded at the first and second scattering orders. Dashed lines indicate the expected positions of Mo(110) and Ni(111) or Mo(220) and Ni(222) bulk reflections.

For the as-grown samples, the relative expansion of $\overline{d}$ (Fig. 5) suggests that the layers are under a global compressive stress state, even at high Λ. In previous studies, an abrupt increase of $\overline{d}$ was observed with decreasing Λ in the range 2–20 nm (see the inset in Fig. 5). In the present case, a slight but monotonic increase is observed with decreasing Λ. Moreover, the evolution is not correlated with the huge elastic softening in the shear modulus (Fig. 2).

Figure 6 shows a strong difference in the structural characteristics of both materials. A significant decrease of d_{Mo} is clearly observed for $\Lambda < 20$ nm. On the other hand, a small change in d_{Ni} is only observed for $\Lambda < 6$ nm. The reduction of d_{Mo} with decreasing Λ may appear quite striking, since, intuitively, one would expect an increase due to the enhancement of coherency stresses at small Λ, owing to the epitaxial relationship between the two lattices.[45]

The distinct evolutions of d_{Mo}, d_{Ni}, and $\overline{d}$ deserve some discussion: only d_{Mo} exhibits a strong evolution while neither d_{Ni} nor $\overline{d}$ show any similar behavior. This implies that the ratio of the number of atomic planes per layer $N_{\mathrm{Mo}}/N_{\mathrm{Ni}}$ deviates from the nominal value. Figure 7 shows the number of planes in the Mo layers extracted from the XRD analysis ($\mathrm{N_{Mo}}$), as a function of the nominal values deduced from the global composition of the multilayers ($\mathrm{N_{Mo}^{nom}}$). Data are reported for Λ in the 4.3–10.8 nm range, for which a consistent refinement of the structural parameters was possible. Experimental points are clearly aligned on a straight line, parallel to the $\mathrm{N_{Mo}}=\mathrm{N_{Mo}^{nom}}$ line, but shifted towards higher values. This constant shift corresponds to ~1.5 monolayers (ML). This means that the Mo layers are thicker than expected; symmetrically, the Ni layers are thinner. Accordingly, this indicates that a constant amount of Ni is incorporated into the Mo layers, at least for this Λ range. This result supports the assumption previously put forward that a mixed NiMo layer is formed during deposition.[33] The origin of this interfacial mixing will be discussed later.

B. Low dose ion irradiation: Stress relaxation

Ion irradiation was performed with 380 keV Ar ions to a fluence as low as $7\times10^{13}/\mathrm{cm}^2$. Atomic rearrangements in the displacement cascades due to the high density of recoil displacements and subsequent Frenkel pair recombination are able to trigger stress relaxation in metallic multilayered films. No significant interdiffusion is expected for such ion doses. Indeed, from SRIM calculations, the spread of the interface can be estimated to only ~1 ML. Therefore, this possibility offers an interesting means to investigate the respective influence of stress on the elastic properties of multilayers.

Asymmetric XRD measurements using the $\sin^2\Psi$ method were performed on some irradiated multilayers.[45] We observed that the elastic strain was almost entirely relaxed in this low-dose irradiation regime. Therefore, the out-of-plane interplanar distances determined from XRD analysis on the irradiated samples may be considered as stress-free lattice spacings. This is clearly visible in Fig. 5: the values of $\overline{d}$ after low-dose ion irradiation are equal, within the limit of experimental uncertainties, to the expected one.

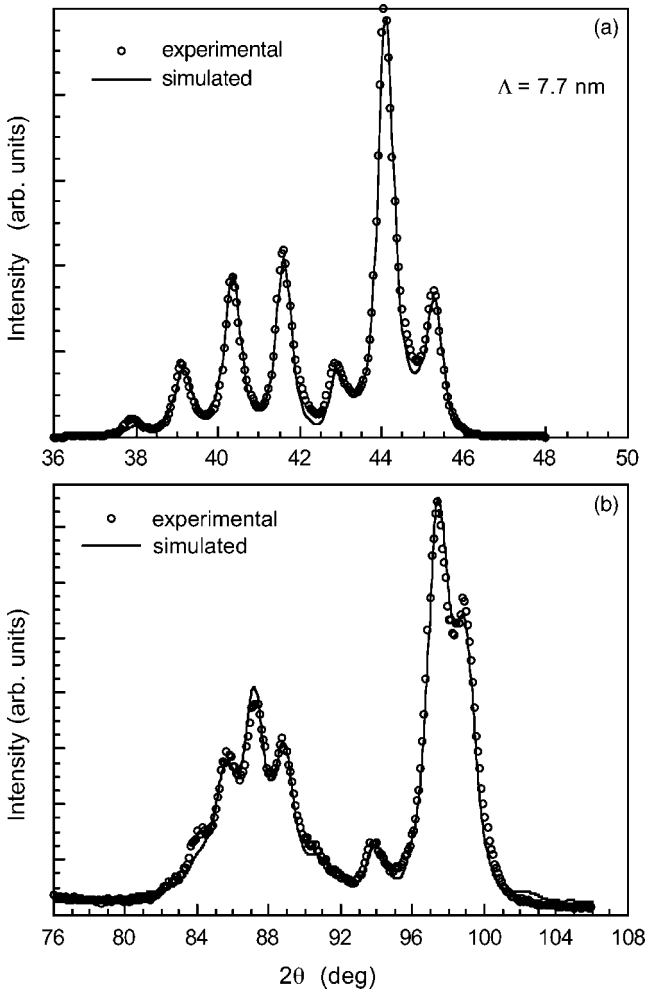

FIG. 4. Experimental high-angle θ-2θ XRD scans (symbols) and refined calculations (solid lines) of an as-grown Ni/Mo multilayer with a bilayer period $\Lambda = 7.7$ nm. On the upper part is shown the profile recorded at the first scattering order (a) and on the lower part at the second order (b).

Figure 8 shows the evolution of XRD $\theta-2\theta$ scans of a multilayer with $\Lambda = 7.7$ nm before and after ion irradiation at a fluence of 7×10^{13} Ar/cm^2. A shift of the Mo envelope position towards higher angles is clearly visible, particularly at the second order, contrarily to the Ni position that remains almost constant. The spectra have been analyzed following the procedure described above. The values of d_{Mo} and d_{Ni} after ion-induced stress relaxation are reported in Fig. 6. As expected from the observed changes of XRD scans, d_{Mo} is found to decrease after ion irradiation, while d_{Ni} remains unchanged. However, the global shape of the evolution of d_{Mo} and d_{Ni} with Λ is unaltered. This suggests that no significant mixing had occurred in this fluence range, at least for $\Lambda > 4.3$ nm for which quantitative information could be extracted from the XRD analysis. Therefore, ion-induced Ni diffusion in the Mo sublayers may be disregarded. It is interesting to notice that, for large values of Λ, d_{Mo} drops down to a value close to the bulk value, confirming that elastic strains originating from residual stresses have been mainly relaxed. For $\Lambda < 20$ nm, d_{Mo} becomes smaller than the bulk value, while d_{Ni} appears slightly higher than the bulk one only for

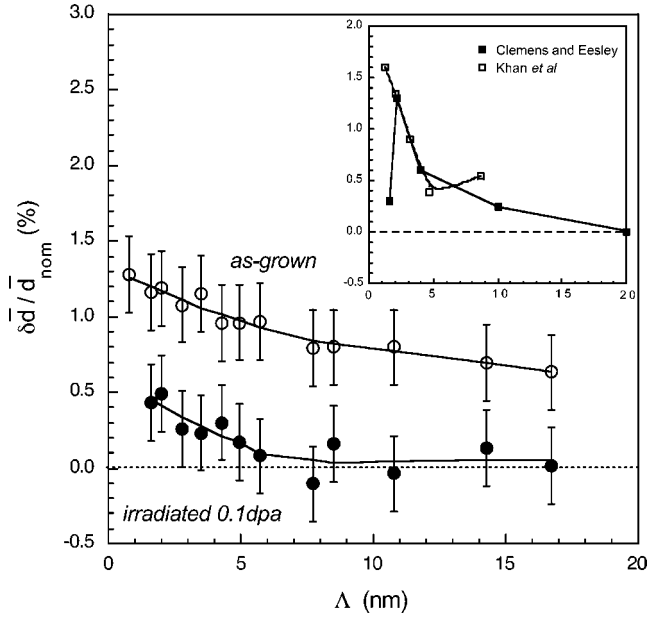

FIG. 5. Out-of-plane average lattice spacing changes $\delta\bar{d}/\bar{d}_{nom}$ as a function of Λ. The open circles correspond to the as-grown multilayers and the filled circles to the same multilayers irradiated at a low ion fluence of 7×10^{13} Ar/cm^2 (0.1 dpa). Also shown in the insert is a comparison with data of the literature (Refs. 10 and 12), for which larger changes were evidenced. The solid lines are only guides for the eyes.

$\Lambda < 7$ nm. This anomalous behavior of d_{Mo} and d_{Ni} for small Λ cannot be attributed to a stress effect, since their variation with Λ remains similar after ion irradiation. Thus, it may be concluded that the variations of d_{Mo} and d_{Ni} observed at small Λ originate from an intermixing effect, which could be ascribed to a chemical interdiffusion occurring during the growth at the Ni/Mo or/and Mo/Ni interface.

If we assume that the intermixed layer thickness is the same for all Λ, its influence will be greater for small Λ values due to the larger interface density. Figure 9 shows that the relaxed lattice parameter scales linearly with the interface density, supporting the idea of an intermixing process. Indeed, such a dependence is expected as much as the thickness of the intermixed layer is smaller than the sublayer thickness. Assuming that the reduction of d_{Mo} is caused by the presence of Ni atoms in the Mo sublattice, the average Ni concentration in the Mo layers, x_{Ni} may be estimated by referring to the best linear laws fitting the measured lattice parameters determined for metastable Ni-rich and Mo-rich Mo_xNi_{1-x} solid-solution sputtered thin films.[45] The Ni average content can be estimated to $\sim$24% for $\Lambda = 4.9$ nm and would reach 50% for $\Lambda \sim 2.5$ nm. If we convert these concentrations in terms of equivalent mass transfer of Ni atoms, one obtains a constant value of 1.5–2 equivalent Ni ML, whatever the Mo thickness. This value is in a rather good agreement with the one deduced from Fig. 7.

The C_{44} elastic constants measured by BLS on the ion-irradiated samples are reported in Fig. 2. Since no stiffening of C_{44} is observed after stress relaxation, the present data demonstrate that elastic strains are not responsible for the huge elastic softening observed at small Λ, as stated

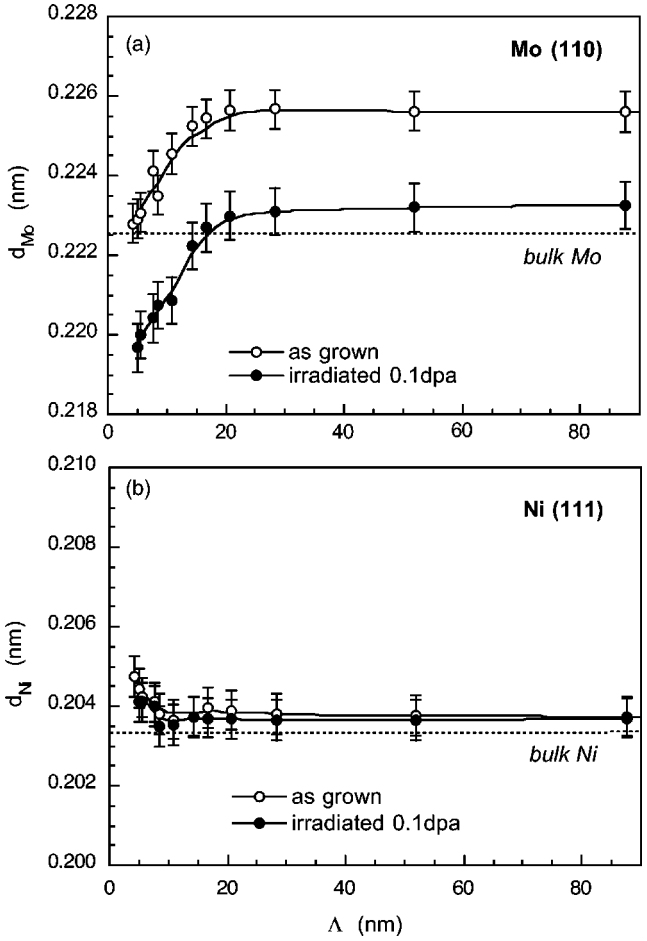

FIG. 6. Interplanar lattice spacing of Mo (a) and Ni (b) layers obtained from the refinement procedure of the XRD spectra. The open circles correspond to the as-grown multilayers and the filled circles to the irradiated ones after a low ion fluence of 7×10^{13} Ar/cm^2(0.1 dpa). The horizontal dashed lines correspond to the bulk values.

previously.[10,12,13] This result also differs from the observations reported by Hues *et al.* in Ag/Co multilayers irradiated with 6 MeV C ions, where a hardening of the shear elastic constant was seen with increasing dose.[46] These authors suggested that this effect was related to a strain release. However, the evolution of XRD patterns rather suggests a slight destratification to occur in this immiscible system.

There were attempts to use thermal treatment[47–49] to design structural changes, but destratification and grain growth did occur, preventing clear conclusions on the elastic properties of the multilayered systems. An essential feature of the ion irradiation technique is that it allows inducing atomic rearrangements and exchanges in a semicontrolled way. To illustrate this point, we have performed XRR experiments on the *same* sample ($\Lambda=4.9$ nm) before and after irradiation. The spectra shown in Fig. 10 are very similar: no significant roughening effect is observed and the bilayer period, Λ, remains unchanged. Since a strong decrease of d_{Mo} is concurrently observed, then this result suggests that an anisotropic stress-driven atomic transport along the growth direction of the multilayer occurs during the ion-induced stress relief stage.

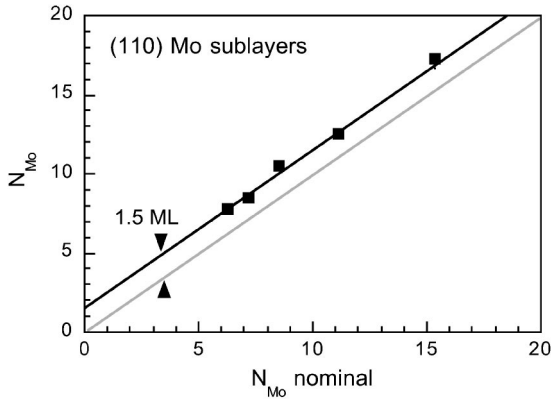

FIG. 7. Number of atomic planes in the Mo layers (N_{Mo}) deduced from the structural refinement procedure, as a function of the nominal expected value. The shift of the straight line towards larger values indicates a transfer of 1.5 ML from the Ni to the Mo layer.

C. High-dose irradiation: Ion mixing

Ion-irradiation was pursued up to large doses on three multilayers samples having different bilayer periods: $\Lambda=2.8$, 7.7, and 28.4 nm. The induced structural changes were deduced from the evolution of the $\theta-2\theta$ XRD scans, while the elastic properties were determined from BLS measurements after successive irradiation doses. In order to compare the elastic behavior of the selected multilayers, we will use in the following the normalized dose $\alpha_{norm}=(\phi/\Lambda^2)^{1/2}$, which characterizes also the mixing yield. This allows us to compare the elastic properties for equivalent mixing yields, since ballistic mixing models as well as radiation-enhanced diffusion ones predict interface spread to increase as the square root of the ion fluence.

1. Structural changes

Selected XRD $\theta-2\theta$ scans recorded on the irradiated samples are shown in Fig. 11. These scans are representative of the four observed different stages, hereafter labeled from 0 to 3. Stage 0, for values of the normalized dose $\alpha_{norm}<0.1$ ion$^{1/2}$/nm^2, corresponds to the ion-induced stress relaxation described in the preceding section.

In stage 1 ($0.1<\alpha_{norm}<0.25$ ion$^{1/2}$/nm^2), ion-induced mixing is clearly evidenced from the evolution of the XRD profiles. For the two multilayers with $\Lambda=2.8$ and 7.7 nm, a significant change in the relative intensities of the superlattice peaks is noticed, leading to the enhancement of the zero-order peak. For $\Lambda=2.8$ nm, due to the limited number of satellite reflections, no information on the composition profile could be extracted. At variance, for multilayers with $\Lambda=7.7$ and 28.4 nm, the mixing may be mainly detected from the change in angular position of the Mo and Ni envelope function. This is clearly visible on the XRD scans of the multilayer with $\Lambda=28.4$ nm recorded both at the first and second orders. A significant decrease of d_{Mo} is deduced from the shift of the Mo(220) Laue function towards high angles, which is attributed to interdiffusion of Ni in the Mo sublayers. Concurrently, an increase of d_{Ni} is observed, owing to interdiffusion of Mo in the Ni sublayers. The evolutions with

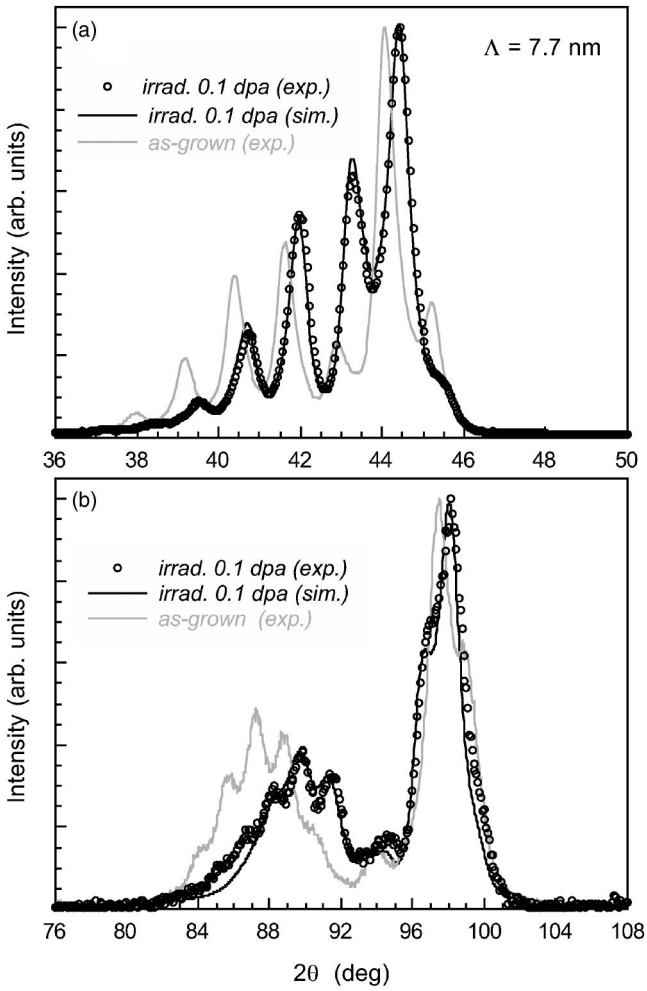

FIG. 8. Experimental high-angle θ-2θ XRD scans (symbols) and refined calculations (solid lines) of an irradiated Ni/Mo multilayer ($\Lambda = 7.7$ nm) with a low ion fluence 7×10^{13} Ar/cm^2 (0.1 dpa). On the upper part are shown the profiles taken at the first scattering order (a) and on the lower part at the second order (b). The experimental profiles of the as-frown multilayer are shown for comparison (gray lines).

$\phi^{1/2}$ (or also with α_{norm}) of the lattice spacings, d_{Mo} and d_{Ni}, deduced from the analysis for the multilayer with $\Lambda = 28.4$ nm are reported in Fig. 12 in a significant dose range. The corresponding ion-induced solubilities in the two elemental sublayers are also shown by referring to measured lattice parameters determined for metastable Ni-rich and Mo-rich solid-solution sputtered thin films.[45]

In stage 2 ($0.25 < \alpha_{\mathrm{norm}} < 1$ ion$^{1/2}$/nm^2), a significant and rather abrupt loss of coherency is detected from the large broadening of the superlattice peaks for the multilayers with $\Lambda = 7.7$ and 28.4 nm. In this stage, no change is observed in the angular position of the Mo envelope and we even observe a quasicomplete disappearance of the Mo envelope with increasing dose. Concomitantly, an angular shift of the Ni(111) envelope towards lower angles is observed, showing that atomic mixing continues by atomic motion of Mo atoms in the Ni sublayers. These observations suggest that the ion-induced solubility of Ni in the Mo sublayers reaches an upper limit above which a strong atomic disordering or even

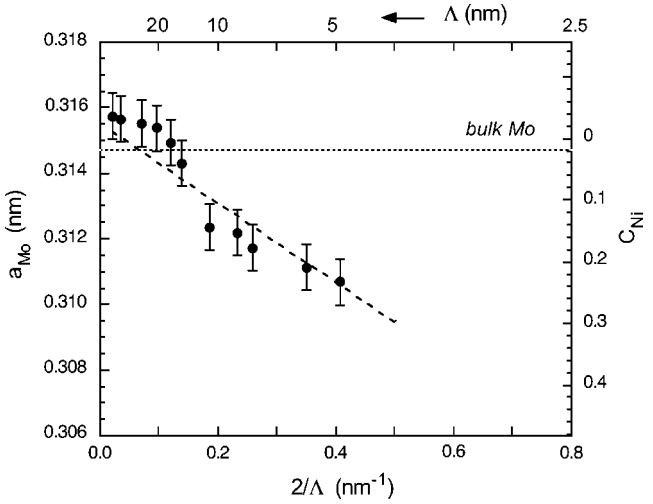

FIG. 9. Unstrained lattice parameter of Mo(110) layers measured after ion-induced stress relaxation as a function of the interface density ($2/\Lambda$). The corresponding average Ni concentration derived from these data using the best linear fit to the lattice parameters of terminal solid solutions Mo_xNi_{1-x} (cf. text) is shown on the right scale.

possibly a bcc to fcc transition takes place. Nevertheless, it may be inferred that no crystalline-to-amorphous transition occurs during the ion-induced interdiffusion process. Indeed, the amorphization of a mixed layer with a spread of only 1 monolayer (ML) would involve the loss of coherency in the x-ray scattering, which in turn would lead to the complete disappearance of satellite peaks.

Finally, in stage 3 ($\alpha_{\mathrm{norm}} > 1$ ion$^{1/2}$/nm^2), the observed XRD profiles attest to the presence of a single-phase alloy, suggesting the complete disappearance of the interfaces and the stabilization of a homogeneous solid solution. The lattice parameter deduced from the observed Bragg reflection near $2\theta \sim 43°$ is consistent with that obtained for a Mo_xNi_{1-x} solid

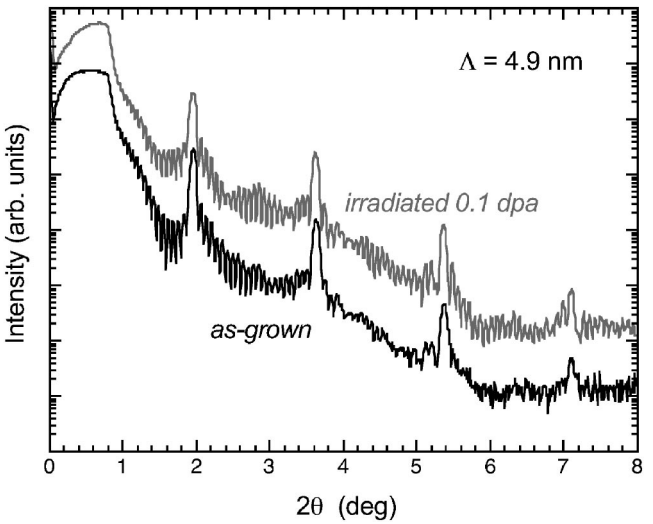

FIG. 10. Specular x-ray reflectivity (XRR) spectra of the as-grown multilayer with $\Lambda = 4.9$ nm before (lower curve) and after irradiation with a low ion fluence (upper curve). The irradiated XRR spectrum is offset by one decade for clarity.

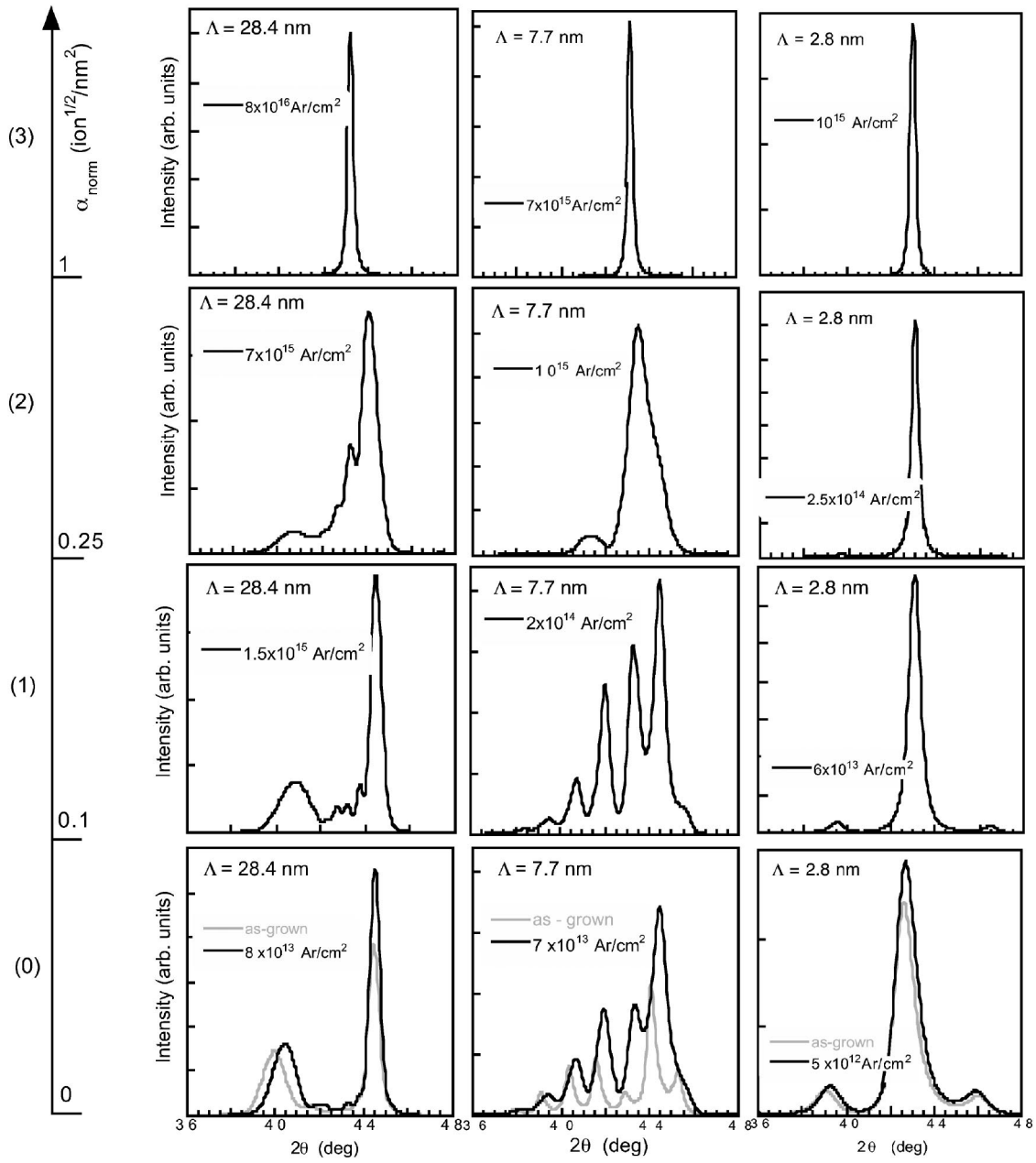

FIG. 11. Evolution of high-angle symmetric θ-2θ XRD scans with the irradiation ion fluence for three representative Ni(111)/Mo(110) superlattices with $\Lambda = 28.4$ nm, 7.7 nm, and 2.8 nm (from left to right). The selected profiles illustrate the distinct mixing stages noted as (0), (1), (2) and (3) observed versus the normalized dose α_{norm} (cf. text).

solution thin film with $x \sim 0.25$, obtained by co-sputtering.[45]

To summarize, several dominant features concerning the mixing process have been seen:

(a) In the first stages, stress relaxation of the Mo sublayers and ion-induced interfacial atomic transport are clearly seen. The solubility of Ni in the Mo sublayers increases as $\phi^{1/2}$, in good agreement with a diffusional process.

(b) For a Ni average solubility threshold of ~0.18, a strong atomic disordering is observed in the Mo sublayers. Subsequently, atomic transport becomes highly asymmetrical favoring the long-range diffusion of Mo in the Ni sublayers. This contrasts with the rather symmetrical profiles predicted from collisional simulations. It is worth noting that the Ni solubility limit observed during the mixing process is close to the critical Ni atomic fraction threshold ($x^{\text{crit}} = 0.27$) above which an amorphous phase is observed in co-sputtered Mo_xNi_{1-x} alloys.[33]

(c) The mixing process leads eventually to the formation of a homogeneous Mo-Ni solid solution, without any intermediate amorphous state. Therefore, the interfaces seem to act as a nucleation barrier to the crystalline-to-amorphous transition.

These results suggest, that in addition to a ballistic flux, *chemically guided atomic transport* also occurs during the ion-irradiation process. This will be discussed in Sec. IV.

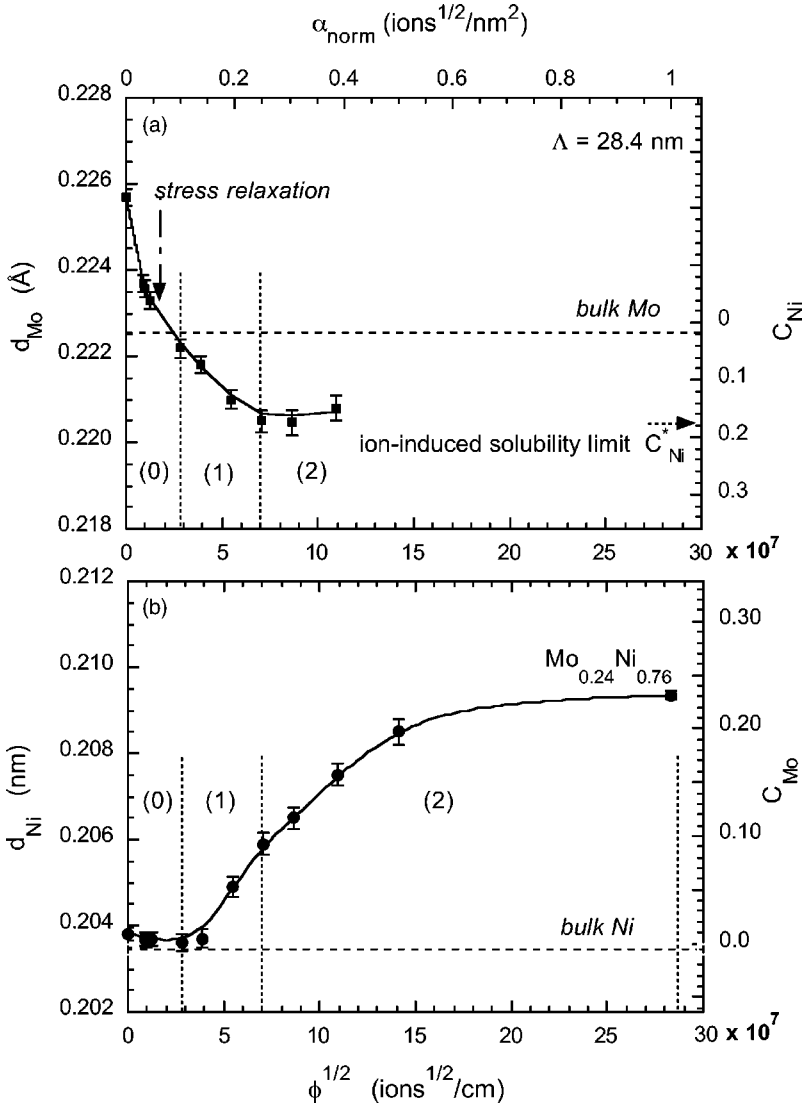

FIG. 12. Average out-of-plane interplanar spacings of (110)Mo (a) and (111)Ni (b) sublayers of a Ni/Mo superlattice with $\Lambda = 28.4$ nm irradiated with 380 keV Ar ions as a function of the square root of the ion fluence $\phi^{1/2}$ [also shown on the top scale is the corresponding normalized dose $\alpha_{norm} = (\phi/\Lambda^2)^{1/2}$]. The corresponding ion-induced Ni(Mo) and Mo(Ni) average concentrations derived from these data are indicated on the right scale. The solid lines are drawn to guide the eyes.

2. Elastic response

A monotonic but distinct evolution of the elastic properties under ionirradiation is observed for the three multilayers (see Fig. 13). A remarkable result is that a common C_{44} value of $\sim$50 GPa is obtained in the final stage, whatever the nominal Λ is. This result is consistent with the formation of a final homogenous solid solution. It is interesting to notice that this value is close to that measured for a metastable fcc $Ni_{0.75}Mo_{0.25}$ crystalline solid solution obtained by co-sputtering.[33] However, it is 38% lower than that of an ideal $Ni_{0.75}Mo_{0.25}$ solid solution ($C_{44} = 81$ GPa), calculated by assuming a rule of weighted average from pure Ni and Mo elastic constants.

A drastic hardening of the C_{44} elastic constant is found for the multilayer with $\Lambda = 2.8$ nm (as shown in Fig. 1 from the gradual frequency shift of the Rayleigh surface mode with increasing ion fluence), while a pronounced softening takes place for the multilayer with $\Lambda = 28.4$ nm, and no significant change is observed for $\Lambda = 7.7$ nm. At first sight, such opposite behaviors would suggest that a clear interdependence between the effective elastic properties and ion mixing does not exist. However, it is noteworthy to remember that elastic constants reflect the strength of the atomic bonding and, accordingly characterize the stability of the system. In this regard, the observed changes in the mechanical properties can be explained in light of the ion-induced structural changes described above. Thus, irradiation of the multilayer with $\Lambda = 2.8$ nm, for which the growth-induced intermixed layer dominates the effective elastic response of the system, induces a significant hardening at the first stages of the mixing process. This trend can be consistently interpreted by assuming a destabilization of the growth-induced supersaturated interfacial-alloyed layer under irradiation, due to chemically guided atomic transport. This is consistent with a mixing evolution path where, not only *random ballistic* motion but also *chemically guided* atomic transport occur, which tend to smear out the locally strong chemical potential gradient present in the intermixed layers, biasing accordingly the stabilization of phases characterized by high free enthalpies (amorphous phase or supersaturated solid solutions), that may trigger a mechanical collapse of the system.

In the multilayer with large Λ, which consists mainly in the as-grown state in pure Mo and Ni layers, the progressive

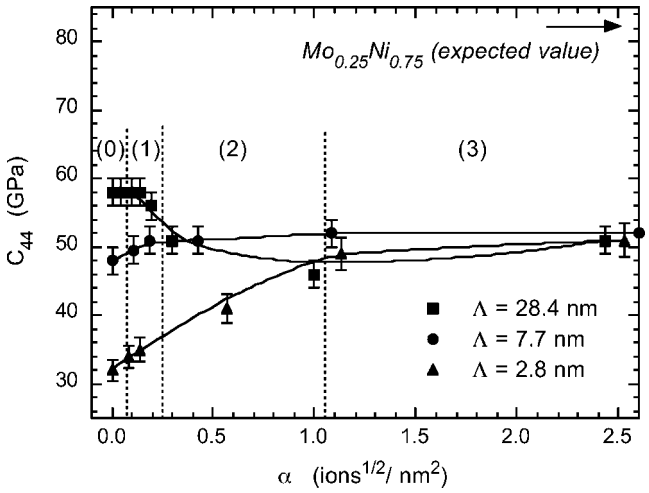

FIG. 13. Dependence of the shear elastic constant on the normalized dose $\alpha_{\mathrm{norm}}=(\phi/\Lambda^2)^{1/2}$ for Ni/Mo multilayers with $\Lambda=2.8$ nm, 7.7 nm, and 28.4 nm. The solid lines are drawn to guide the eyes.

C_{44} softening is mainly dominated by the mixing process in the volume layers. The interfaces will only marginally influence the total evolution until the formation of a complete solid solution. The lack of change under irradiation in the elastic properties of the multilayer with $\Lambda=7.7$ nm is probably quite fortuitous and would be the result of a balance between the two different mixing processes. Conversely, the influence of the ion irradiation on the elastic properties of the multilayers with ultra thin layer thickness entirely supports the existence in the as-grown state of a strong interfacial chemical gradient involving metastable supersaturated solid solutions and its destabilization under irradiation.

IV. DISCUSSION

A. Interfacial mixing: Segregation effects

The analysis of the XRD spectra recorded on the as-deposited and irradiated multilayers reveals the presence of an asymmetrical mixing in the as-deposited Mo/Ni multilayers, with a preferential diffusion of Ni in the Mo sublayers. The concentration gradient at the interface leads to the formation of metastable and supersaturated solid solutions. The issue of interfacial mixing is of great importance in multilayers, especially in nanoscale systems. Nonequilibrium structures and new phases can be stabilized during growth. As shown here, the presence of such structures has a marked consequence on the effective elastic properties of the multilayers. This concerns especially the C_{44} and C_{33} effective elastic constants, which are very sensitive to interfacial effects, compared to other effective elastic constants (C_{11},C_{12},C_{22}).[40]

In the bulk state, the Ni-Mo equilibrium phase diagram exhibits only a few intermetallic compounds and terminal solid solutions with a very limited solubility, even at high temperatures.[50] For instance, for the Mo-rich side the maximal solubility limit is only 1.8% for $T>1646$ K and $\sim 0\%$ at RT. However, it is well recognized that the formation of nonequilibrium phases generally takes place at the growth front, where dynamical segregation effects may occur. Consequently, the driving force for stabilization is therefore supplied by a lowering of surface or interface energies. Asymmetrical interfacial mixing has already been seen in several metallic multilayers, e.g., Au/Ni,[51–54] Co/Sb,[55] and explained by the surfactant nature of one element during the growth due to enhanced surface mobility.[56] In the present system, the calculated surface energy for Ni(111) and Mo(110) planes are 1.44 and 1.83 $\mathrm{J/m^2}$, respectively.[57,58] Such a small difference in surface energies cannot solely account for the observed dynamic segregation in the Mo/Ni system. Interface energy also plays an important role for very thin layers. A strong chemical bonding or a misfit strain relaxation due to intermixing could favor the lowering of the interface energy, as reported in the Fe/Pt system.[59] The propensity for epitaxial growth between Ni and Mo is undeniably related to the strength of the Ni-Mo bonding. Although the contribution of the bulk chemical mixing enthalpy is positive, the overall free energy of the supersaturated interfacial layer, including interfacial and elastic contributions, may become negative. The large strains and the tendency of the adatoms to avoid some unfavorable positions may therefore promote exchange mechanisms.[60] Various mechanisms for the formation of interfacial alloys have been put forward from recent molecular dynamics simulations. In the case of Co on Cu, Stepanyuk *et al.*[61] found that, due to the inhomogeneous stress distribution related to heteroepitaxy, the vacancy activation energy was drastically reduced near the cluster edges. Such a mechanism may promote burrowing of Co clusters on Cu(001), as recently observed by Zimmermann *et al.*[62] At variance, in the case of Pt on Co (compressive islands), Goyhennex *et al.*[63] pointed out an ejection of the Co atoms near the coalescence threshold between islands, according to a "fountain effect." Both mechanisms are triggered by the occurrence of large stress distributions. Therefore, accounting for the large lattice mismatch between Mo and Ni (9% by referring to the distances between neighboring atoms), such mechanisms could explain the intermixing in strained Ni/Mo superlattices. Obviously, these atomic rearrangements will only occur under enhanced surface mobility conditions, e.g., for low deposition rate, high temperature, or energetic incident particles.

In the case of ion beam sputtering, sputtered atoms are highly energetic. Estimation of the adatom energy distributions, using SRIM simulations,[36] gives mean values of 30 and 18 eV for Mo and Ni, respectively, but with a long tail extending to the hundreds of eV. Although numerous experimental studies attest to the formation of a high concentration of defects and related specific growth stresses for $T<0.25T_m$ (T_m being the melting temperature), the exact mechanisms of their production in this energy range and in the near-surface region are not yet fully understood.[64] Molecular dynamics simulations show, however, that self-interstitials are formed by focused replacement collision sequences in close-packed directions at depths beyond 4 ML, whereas vacancies annihilate at the surface.[65,66] Therefore, the influence of such high concentrations of defects on the formation and stability of nonequilibrium interfacial structures remains to be established. To address this issue, de-

tailed comparative studies on multilayers grown by thermal vapor deposition and ion beam sputtering need to be carried out. Finally, one cannot ignore direct ballistic effects, such as forward recoils, but their contribution does not allow to explain the asymmetrical mixing.

B. Ion-induced stress relaxation and mixing

The originality of the present study lies in the use of energetic heavy ions in the keV range to induce, in a semi-controlled way, structural modifications and to study their relationship with elastic properties. There is a clear difference between the effects of such irradiations and those induced by incoming sputtered atoms, since the transferred energy and affected depths differ by 2–3 orders of magnitude. The keV heavy ions are mainly slowed down in the multilayered film by two processes: electronic excitations and elastic collisions with the lattice atoms. This last contribution dominates the irradiation-induced effects, in particular for metallic systems. Moreover, since the typical transferred energies to the primary recoil atoms are large ($\sim$10 keV range), an increasing number of atoms are displaced locally in displacement cascades distributed all along the ion path. Vacancies and interstitials are produced, but defect clusters or complexes may also be formed. Spontaneous vacancy-interstitial recombination may occur if the separation distance between a vacancy and an interstitial is not too large (typically several atomic distances). In addition to defect production, several non equilibrium or equilibrium processes may occur: ballistic mixing, lattice disordering and, depending on the temperature, enhanced atomic mobility. Thus, opposite consequences can be observed and the dominating effect depends on the irradiation conditions (energy, ion mass, temperature and related cascade size and density, atomic mobility) and also on the thermodynamics of the system.

One illustration of this concerns the irradiation effects induced at RT by 380 keV Ar ions in a Mo(110) sputtered thin film. Preliminary measurements show that atomic displacements and related rearrangements induced in the displacement cascades trigger a relaxation of the growth-induced stresses.[67] Ion-induced stress relaxation begins at the very first stages of the irradiation (doses <0.01 dpa) and is achieved at $\sim$0.1 dpa. Therefore cascade overlapping does not seem to be required. Caution should be paid, however, for multilayers with ultrathin constituent layers, since mixing effects cannot be entirely disregarded, even at low-dose regimes. Furthermore, a proper analysis of the residual strain and stress fields present in these multilayers should be carried out to support these results and also to investigate the mechanisms of the ion-induced stress relaxation. Such a detailed study is in progress in epitaxial Mo(110)/Ni(111) multilayers grown onto Al_2O_3 $[1\bar{1}20]$ substrates.[45,68]

Another notable result is the interplay between ion mixing effects and elastic properties. Indeed, the interdependence between the ion-induced elastic changes—stiffening or softening, depending on Λ—and mixing supports the idea of an atomic mixing driven by both ballistic effects and chemically guided defect motion. Thus, for given irradiation conditions, the dynamic evolution path of this "driven" system is governed by thermodynamics, as predicted within the theoretical framework of Martin and Bellon.[69,70] This trend is more especially seen for very thin layers: the spread of the interfacial gradient due to chemically guided atomic motion dominates the structural and mechanical evolution of the system. Starting from an initial state very far from equilibrium, the system evolves—when submitted to external forcing conditions (ion irradiation)—towards metastable and relaxed macroconfigurations.

From a more fundamental point of view, the present data shed some light on the understanding of phase transformation in driven alloys and related chemically guided atomic diffusion. Chemical guidance and related high mixing efficiencies observed in some metallic systems (Au, Cu, etc.) are generally explained within the so-called thermal spike model, i.e. by involving transient and high-temperature regimes in the core of the cascades.[71,72] Such effects are not expected in this system. Indeed, it has been shown from molecular dynamics simulations that thermodynamic properties—more especially temperature and thermal diffusivity—appear unfavorable to the formation of a thermal spike in a refractory metal such as Mo or even Ni.[73] However, it is also possible to take the chemical effects into account in a different approach, where the dominant mixing mechanism is of ballistic nature but where isolated defects are mobile at the irradiation temperature, after cascade cooling. Using such an approach, a "chemically guided" atomic flux may be derived, which represents the product of the defect mobility by the gradient of the chemical potential. Accordingly, such an additional atomic flux tends to erase strong chemical potential gradients and may be efficient even at low temperature. Thus, Kelly and Miotello[74] demonstrated that the diffusion profile is severely influenced, even when the ratio of the diffusivities for chemically guided defect motion to random one lies in the interval 0.01–0.1. Moreover, they observed the occurrence of a miscibility gap at the interface in systems with large positive mixing enthalpy. This defines an ion-induced solubility limit larger than the equilibrium one. In the present case, positive values of mixing enthalpies for fcc and cc solid solutions of 3.2 and 20.9 kJ/mol, respectively, are estimated following the semi-empirical description of de Boer *et al.*[75] So, such an approach constitutes a satisfactory framework to account for the peculiar behavior exhibited in the Ni/Mo multilayers, i.e., a miscibility-gap-like occurrence and the highly asymmetrical atomic flux observed in the last mixing stage. Obviously, the induced-solubility limit may depend on the given forcing conditions (380 keV Ar ions, RT) and sample characteristics (here, layer thickness ratio). Last, since only self-interstitials are mobile at the temperature of our experiments (300 K), then our results give clear indication that interstitial motion is at least in part chemically guided. Such an effect has been put forward to explain radiation-induced segregation in the low temperature range[76] but, comparatively not often invoked to account for chemical effects in ion beam mixing.[77]

V. CONCLUSION

In summary, the interdependence between structural and elastic properties of Ni(111)/Mo(110) multilayers in the as-

deposited state and after ion-induced stress relaxation was investigated for a large Λ range (0.8–87.5 nm). BLS measurements show that a drastic softening of the effective shear modulus occurs with decreasing Λ, until $\Lambda = 2$ nm where it reaches −62%. XRD analysis reveals that the overall expansion of the average lattice spacing $\bar{d}$ is period independent. Ion irradiation in a medium-energy range (380 keV) and at relatively low dose (~0.1 dpa) releases the lattice expansion and associated compressive stresses. However, no stiffening of the elastic response is observed, which indicates that the elastic behavior of these multilayers is not correlated with the presence of elastic strains.

Analysis of the XRD θ–2θ scans after ion-induced stress relief reveals a pronounced decrease of d_{Mo} below the bulk value as Λ decreases. Moreover, the unstrained lattice parameter of Mo layers exhibit a remarkable linear dependence with the interface density, while the Ni unstrained lattice parameter remains unchanged in the same Λ range. The most likely explanation for these observations is that a constant Ni amount (~1.5 ML) substantially intermixes into the Mo layers during deposition. This interfacial mixing is a consequence of the dynamic segregation of Ni atoms during growth and leads to an average Ni concentration in the Mo sublayers of up to 50 % in the Λ range where the shear elastic constant is drastically lessened. Thus, the formation of interfacial metastable and supersaturated solid solutions, structurally and mechanically unstable, appears as the origin of the large elastic softening observed in this system.

At high ion fluences, when the mixing process becomes dominant, irradiation reveals the complex interplay between ion mixing effects and elastic properties. Ion-induced elastic changes—stiffening or softening, depending on Λ—and mixing are observed. A full understanding of such irradiation-induced effects requires implementation of thermodynamics. Thus, while atomic mixing is triggered by ballistic effects (i.e. random motion), a chemically guided atomic motion must be involved to account for the specific features of the atomic transport, i.e., both the solubility limit of Ni in Mo sublayers, indicating the appearance under irradiation of a miscibility-gap-like phenomenon, and the subsequent asymmetrical atomic transport. Accordingly, depending on the yield of the initial interfacial chemical gradient to the layer thickness, chemical guided atomic motion or ballistic mixing influences more or less efficiently the effective elastic response leading the system towards the more stable (structurally and mechanically) steady state.

ACKNOWLEDGMENTS

The authors gratefully acknowledge the assistance of Ph. Guerin and M. Drouet in sample preparation and irradiation experiments. This work was supported by the French Ministry of Research under ACI "Surfaces, Interfaces and Conception of New Materials", project "DELTAMU" No. S39-01.

*Corresponding author. Electronic address: christiane.jaouen@univ-poitiers.fr
†Present address: Laboratoire des Milieux Désordonnés et Hétérogènes, UMR CNRS 7603, Université Pierre et Marie Curie, 4 Place Jussieu, 75252 Paris Cedex 05, France.

[1] I. K. Schuller, A. Fartash, and M. Grimsditch, MRS Bull. **15**(10), 33 (1990).
[2] A. F. Jankowski, Nanostruct. Mater. **6**, 179 (1995).
[3] W. M. C. Yang, T. Tsakalakos, and J. E. Hilliard, J. Appl. Phys. **48**, 876 (1977).
[4] L. R. Testardi, R. M. Willens, J. T. Krause, D. B. Mc Whan, and S. Nakahara, J. Appl. Phys. **52**, 510 (1981).
[5] T. Tsakalakos and J. E. Hilliard, J. Appl. Phys. **54**, 734 (1982).
[6] A. Kueny, M. Grimsditch, K. Miyano, I. Banerjee, C. M. Falco, and I. K. Schuller, Phys. Rev. Lett. **48**, 166 (1982).
[7] J. A. Bell, W. R. Bennet, R. Zanoni, G. I. Stegeman, C. M. Falco, and C. T. Seaton, Solid State Commun. **64**, 1339 (1987).
[8] A. Fartasch, E. E. Fullerton, I. K. Schuller, S. E. Bobbin, J. W. Wagner, R. C. Cammarata, S. Kumar, and M. Grimsditch, Phys. Rev. B **44**, 13 760 (1991).
[9] R. Danner, R. P. Hebener, C. S.L. Chun, M. Grimsditch, and I. K. Schuller, Phys. Rev. B **33**, 3696 (1986).
[10] M. R. Khan, C. S. L. Chun, G. P. Felcher, M. Grimsditch, A. Kueny, C. M. Falco, and I. K. Schuller, Phys. Rev. B **27**, 7186 (1983).
[11] I. K. Schuller and M. Grimsditch, J. Vac. Sci. Technol. B **4**, 1444 (1986).
[12] B. M. Clemens and G. L. Eesley, Phys. Rev. Lett. **61**, 2356 (1988).
[13] G. Richardson, J. L. Makous, H. Y. Yu, and A. S. Edelstein, Phys. Rev. B **45**, 12 114 (1992).
[14] E. E. Fullerton, S. Kumar, M. Grimsditch, D. M. Kelly, and I. K. Schuller, Phys. Rev. B **48**, 2560 (1993).
[15] E. E. Fullerton, I. K. Schuller, F. T. Parker, K. A. Svinarich, G. E. Eesley, R. Bhadra, and M. Grimsditch, J. Appl. Phys. **73**, 7370 (1993).
[16] J. A. Bell, W. R. Bennett, R. Zanoni, G. I. Stegeman, C. M. Falco, and F. Nizzoli, Phys. Rev. B **35**, 4127 (1987).
[17] J. R. Dutcher, S. Lee, J. Kim, A. Bell, G. I. Stegeman, and C. M. Falco, Mater. Sci. Eng., B **6**, 199 (1990).
[18] G. Carlotti, D. Fioretto, G. Socino, B. Rodmacq, and V. Pelosin, J. Appl. Phys. **71**, 4897 (1992).
[19] G. Carlotti, A. Montone, C. Petrillo, and M. Vittori Antisari, J. Phys.: Condens. Matter **5**, 4611 (1993).
[20] W. E. Pickett, J. Phys. F: Met. Phys. **12**, 2195 (1982).
[21] T. B. Wu, J. Appl. Phys. **53**, 5265 (1982).
[22] M. L. Hubermann and M. Grimsditch, Phys. Rev. Lett. **62**, 1403 (1989).
[23] R. C. Cammarata and K. Sieradzki, Phys. Rev. Lett. **62**, 2005 (1989).
[24] F. H. Streitz, R. C. Cammarata, and K. Sieradzki, Phys. Rev. B **49**, 10 707 (1994).
[25] A. F. Jankowski and T. Tsakalakos, J. Phys. F: Met. Phys. **15**, 1279 (1985).
[26] A. Banerjea and J. R. Smith, Phys. Rev. B **35**, 5413 (1987).
[27] D. Wolf and J. F. Lutzko, J. Appl. Phys. **66**, 1961 (1989).

[28] J. A. Jaszczak, S. R. Phillipot, and D. Wolf, J. Appl. Phys. **68**, 4573 (1990).
[29] J. A. Jaszczak and D. Wolf, J. Mater. Res. **6**, 1207 (1991).
[30] J. L. Makous and S. Hues, Phys. Rev. B **44**, 10 848 (1991).
[31] I. K. Schuller and A. Rahman, Phys. Rev. Lett. **50**, 1377 (1983).
[32] J. A. Bain, L. J. Chyung, S. Brennan, and B. M. Clemens, Phys. Rev. B **44**, 1184 (1991).
[33] G. Abadias, C. Jaouen, F. Martin, J. Pacaud, Ph. Djemia, and F. Ganot, Phys. Rev. B **65**, 212105 (2002).
[34] E. E. Fullerton, I. K. Schuller, H. Vanderstraeten, and Y. Bruynesaraede, Phys. Rev. B **45**, 9292 (1992).
[35] L. G. Parratt, Phys. Rev. **95**, 359 (1954).
[36] J. F. Ziegler, J. P. Biersack, and U. Littmark, *The Stopping and Range of Ions in Matter* (Pergamon, New York, 1985); http://www.srim.org
[37] P. Lucasson, in *Fundamental Aspects of Radiation Damage in Metals (Gatlinburg, Tennessee, 1975)*, edited by M. T. Robinson and F. W. Young, Jr. (US Energy Research & Development Administration, Conf-751006, National Tech. Inform. Service, Springfield, VA, 1975), p. 42.
[38] M. Jaouen, J. Pacaud, and C. Jaouen, Phys. Rev. B **64**, 144106 (2001).
[39] P. Djemia, Ph.D. thesis, University of Paris Nord, France, 1998.
[40] M. Grimsditch and F. Nizzoli, Phys. Rev. B **33**, 5891 (1986).
[41] R. F. S. Hearmon, in *The Elastic Constants of Non-Piezoelectric Crystals*, edited by K. H. Hellwege and A. M. Hellwege, Landolt-Börnstein, New Series, Group III, Vol. 11 (Springer-Verlag, Berlin, 1969), p. 10.
[42] A. Reuss, Z. Angew. Math. Mech. **9**, 49 (1929).
[43] W. Voigt, *Lehrbuch der Kristallphysik* (Teubner, Leipzig, 1910).
[44] R. Hill, Proc. Phys. Soc., London, Sect. A **65**(5A), 349 (1952).
[45] F. Martin, Ph.D. thesis, University of Poitiers, France, 2003.
[46] S. M. Hues, B. Bhadra, M. Grimsditch, E. Fullerton, and I. K. Schuller, Phys. Rev. B **39**, 12 966 (1989).
[47] B. Hillebrands, P. Krams, K. Sporl, and, D. Weller, J. Appl. Phys. **69**, 938 (1991).
[48] G. Carlotti, D. Fioretto, G. Socino, L. Verdini, and V. Pelosin, J. Appl. Phys. **73**, 3028 (1993).
[49] S. Lee, G. I. Stegeman, J. Kim, M. Falco, V. Askarpour, and M. H. Manghnani, Solid State Commun. **94**, 691 (1995).
[50] T. B. Massalski *et al.*, *Binary Alloy Phase Diagrams*, 2nd ed. (ASM Int.: Materials Park, OH, 1990).
[51] S. P. Baker, J. A. Bain, B. M. Clemens, and W. D. Nix, Mater. Res. Soc. Symp. Proc. **343**, 555 (1994).
[52] P. Bayle, T. Deutsch, B. Gilles, F. Lançon, A. Marty, and J. Thibault, Ultramicroscopy **56**, 94 (1994).
[53] F. Tamisier, Ph.D thesis, University of Poitiers, France, 1997.
[54] S. Labat, P. Gergaud, O. Thomas, B. Gilles, and A. Marty, J. Appl. Phys. **87**, 1172 (2000).
[55] N. Nakayama, K. Takahashi, T. Shinjo, T. Takada, and H. Ichinose, Jpn. J. Appl. Phys., Part 1 **25**, 552 (1986).
[56] J. M. Roussel, A. Saúl, G. Treglia, and B. Legrand, Phys. Rev. B **60**, 13 890 (1999).
[57] P. Gumbsch and M. Daw, Phys. Rev. B **44**, 3934 (1991).
[58] G. J. Ackland and M. W. Finnis, Philos. Mag. A **54**, 301 (1986).
[59] T. C. Hufnagel, M. C. Kautzky, B. J. Daniels, and B. M. Clemens, J. Appl. Phys. **85**, 2609 (1999).
[60] J. Tersoff, Phys. Rev. Lett. **77**, 2017 (1996).
[61] V. S. Stepanyuk, D. I. Bazhanov, A. N. Baranov, W. Hergert, P. H. Dederichs, and J. Kirshner, Phys. Rev. B **62**, 15 398 (2000).
[62] C. G. Zimmermann, M. Yeadon, K. Nodlund, J. M. Gibson, R. S. Averback, U. Herr, and K. Samwer, Phys. Rev. Lett. **83**, 1163 (1999).
[63] C. Goyhennex, H. Bulou, J. P. Deville, and G. Treglia, Phys. Rev. B **60**, 2781 (1999); Appl. Surf. Sci. **177**, 238 (2001).
[64] H. Windischmann, Crit. Rev. Solid State Mater. Sci. **17**, 547 (1992).
[65] F. Karetta and F. M. Urbassek, J. Appl. Phys. **74**, 5410 (1992).
[66] C. M. Gilmore and J. A. Sprague, Thin Solid Films **419**, 18 (2002).
[67] A. Debelle, G. Abadias, A. Michel, and C. Jaouen, Appl. Phys. Lett. **84**, 5034 (2004); A. Debelle, G. Abadias, A. Michel, C. Jaouen, M. Droue, and Ph. Guérin, Mater. Res. Soc. Symp. Proc. **795** U12.3, p 1 (2004).
[68] F. Martin, J. Pacaud, G. Abadias, C. Jaouen, and Ph. Guerin, Appl. Surf. Sci. **188**, 90 (2002).
[69] G. Martin, Phys. Rev. B **30**, 1424 (1984).
[70] G. Martin and P. Bellon, Solid State Phys. **50**, 189 (1997).
[71] W. L. Johnson, Y. T. Cheng, M. Van Rossum, and M-A. Nicolet, Nucl. Instrum. Methods Phys. Res. B **7/8**, 657 (1985).
[72] T. Cheng, Mater. Sci. Rep. **5**, 45 (1990).
[73] T. Diaz de la Rubbia, R. S. Averback, R. S. Hsieh, and R. Benedek, J. Mater. Res. **4**, 579 (1989).
[74] R. Kelly and A. Miotello, Nucl. Instrum. Methods Phys. Res. B **59/60**, 517 (1991); Surf. Coat. Technol. **51**, 343 (1992); Appl. Phys. Lett. **64**, 2649 (1994).
[75] F. R. de Boer, R. Boom, W. C. Mattens, A. R. Miedema, and A. K. Niessen, *Cohesion in Metals* (North-Holland, Amsterdam, 1988).
[76] L. E. Rehn and P. R. Okamoto, J. Nucl. Mater. **78**, 985 (1987).
[77] R. S. Averback, D. Peak, and L. J. Thomson, Appl. Phys. A: Solids Surf. **39**, 59 (1986).